City Research Online

City, University of London Institutional Repository

This is the published version of the paper.

This version of the publication may differ from the final published version.

Permanent repository link: http://openaccess.city.ac.uk/id/eprint/23346/

Link to published version: http://dx.doi.org/10.1364/osac.2.003008

City Research Online: http://openaccess.city.ac.uk/   publications@city.ac.uk

Investigation of a SPR based refractive index sensor using a single mode fiber with a large D shaped microfluidic channel

A. K. PATHAK,[1,3] (iD) **V. K. SINGH,**[1,4] **S. GHOSH,**[2] (iD) **AND B. M. A. RAHMAN**[2,5]

[1]*Optical fiber laboratory, Indian Institute of technology (Indian School of Mines), Jharkhand, India*
[2]*School of Mathematics, Computer Science and Engineering, City, University of London, Northampton Square, London, EC1V 0HB, UK*
[3]*akhileshpathak57@ap.ism.ac.in*
[4]*vksingh@iitism.ac.in*
[5]*b.m.a.rahman@city.ac.uk*

Abstract: In this work, a highly sensitive surface plasmon resonance (SPR) sensor based on a single mode fiber (SMF) incorporating a large microfluidic channel (MFC) for refractive index (RI) sensing is designed and optimized using a full-vectorial finite element method (FEM). The fluidic channel size can be varied according to the requirement due to the availability of the large cladding diameter of SMF, which makes it simple and easy to fabricate. The proposed novel sensor is favourable to both analytes and metallic strips. The D-shaped hollow section above the core is filled with the measurand analytes and a gold (Au) strip is deposited on the base of the MFC, as it is known as the most attractive metal for SPR. Our numerical simulations illustrate that the confinement loss of the designed sensor is highly influenced by the distance of the MFC from the core along with the width and thickness of the Au strip. The designed sensor shows an average sensitivity of 1350 nm/RIU and maximum sensitivity of 8250 nm/RIU in the sensing range of 1.33-1.35 and 1.41-1.43, respectively. However, for a small variation of n_a at a step of 0.005, within ranges like 1.415, 1.420, and 1.425, we have achieved a maximum sensitivity of 7000 nm/RIU, 9000 nm/RIU and 11000 nm/RIU, respectively. This novel SPR sensor with MFC can open up a new opportunity in the application of chemical and biological sensing.

1. Introduction

Over the last few decades, SPR techniques have achieved considerable recognition because of their salient characteristics in term of sensitivity, label-free detection, fast response time and hence offer potential application in the field of chemical and biological sensing. SPR is a unique phenomenon of optical event arises due to the strong collective oscillation of charge density at the interface of metal and dielectric [1]. The surface plasmon polaritons are highly sensitive towards a small change in the surrounding environment [2]. These special features of the SPR technique form the theoretical basic of various designed sensors like pH sensor, RI sensor, temperature sensor, biosensor, etc [3–7].

The conventional SPR sensors based on prism [8] and waveguide technologies [9,10], suffers many drawbacks like bulky in size, high-cost fabrication process, difficult to integrate with the system, hard to carry and too complex to operate. Optical fiber sensors using SPR technique are developed in response to overcome of these drawbacks. SPR based optical fiber sensors play a crucial role over traditional sensors in terms of high sensitivity, lower detection limit, low-cost fabrication, real-time monitoring, immune to electromagnetic interference [11–13] and can be applicable to biochemistry, industrial area and environmental monitoring. In order to design an SPR based optical fiber sensor the core guided light must extend through the fiber to

interact with the metallic coating. There are various sensors designed to achieve this process such as D shaped fibers [14], microstructured optical fibers (MOFs) [15,16] and U bent fiber [17]. Among these reported sensors, *D* shaped polished fiber based sensors are more popular due to their flexibility in altering their mechanical and optical properties for various applications. Sensors based on D shaped structures achieve a high sensitivity and allowed various parameters like strain, temperature, and RI to be waqmeasured accurately [18,19]. In 2015, Patnaik *et al.* introduced an ITO coated D shaped sensor and achieve a high sensitivity of 5700 nm/RIU. Their proposed sensing configuration permit higher interaction of light with outer media due to the polished surface and ITO layer [20]. Later in 2016 Qazi *et al.* proposed a new kind of strain sensor by polishing a standard SMF just above the core [21]. In this work, a D-shaped polarization-maintaining fiber loop mirror sensor for the simultaneous monitoring of strain and temperature is proposed and achieved a high sensitivity of 46 pm/με and 130 pm/°C for strain and temperature, respectively. These examples show that, how the polishing of fiber can enhance the sensitivity of the sensor. All these sensors are fabricated by side-polishing the cladding of fiber along the half of its circumference in order to form it in D shaped structures. Although these sensors achieve high sensitivity in their respective areas, but they face various drawbacks such as it destroys the circular symmetry of optical fiber which results in the additional polarization-based losses [22] also it may leads difficulty in splicing, and become fragile in nature [23,24]. Hence our main motive is to design a robust device which may short out these problems and provide the maximum interaction of light and sensitivity without losing its symmetrical nature.

In the present work, we proposed a newly designed SPR sensor based on D shaped MFC for a wide range of RI sensing. In which a large D shaped MFC is incorporated just above the core in the cladding section to fill analytes of varying RI. The base of MFC is coated with a thin Au strip to enhance the sensitivity and achieve SPR phenomenon. The numerical investigation based on a finite element method (FEM) is carried out here to estimate the performance and the influence of the parameters for the designed sensor. The sensor is based on wavelength modulation technique with a high sensitivity of 8250 nm/RIU for RI range varying between 1.41-1.43, which is higher than other reported papers based on the similar techniques [25–28]. The numerically simulated results indicate that the incorporation of MFC in a SMF may improve the sensitivity compared to the previously reported articles.

2. Structural design and numerical analysis

For the proposed sensor, the substrate is D shaped MFC based SMF. The proposed structure can be fabricated by modified chemical vapor deposition (MCVD) method as reported by Li *et al.* [29]. In which a fiber containing D shaped MFC was first fabricated using modified chemical vapor deposition preform with a flat ground on one side. The separation between the fiber core and the MFC is relevant to the structure parameters of the preform. In order to fabricate a precise and accurate D-shaped preform, the preform with a rough cut is polished to control the residual diameter progressively [30]. Following that the prepared preform was sleeved with a silica tube and drawn into a fiber. It is worthy to note that during the drawing of such fibers, the inert gas replaces the low melting point metals which was pumped in MFC to maintain the shape of MFC. Furthermore, when the temperature and rate of drawing is accurate, we can fabricate an ideal fiber containing D shaped MFC. Figure 1 shows the schematic diagram of the cross-sectional view of the designed sensor. The proposed sensor is designed using standard SMF with core diameter of 9 μm and cladding diameter 125 μm with one-side incorporating a large D-shaped MFC. The RI of Ge doped core and fused silica cladding is obtained by using the Sellmeier equation and can be defined as,

$$n^2(\lambda^2) = 1 + \frac{B_1\lambda^2}{\lambda^2 - C_1} + \frac{B_2\lambda^2}{\lambda^2 - C_2} + \frac{B_3\lambda^2}{\lambda^2 - C_3} \tag{1}$$

where, $B_{1,2,3}$ and $C_{1,2,3}$, are the Sellimeiers coefficients whose values are taken from [31]. For Fused silica the used Sellimeiers coefficients are taken as $B_1 = 0.6961663$, $B_2 = 0.4079426$, $B_3 = 0.8974794$, $C_1 = 0.0684043$, $C_2 = 0.1162414$ and $C_3 = 9.896161$, while for Ge doped core it was chosen as $B_1 = 0.7347008$, $B2 = 0.4461191$, $B_3 = 0.8081698$, $C_1 = 0.0764679$, $C_2 = 0.1246081$ and $C_3 = 9.896203$.
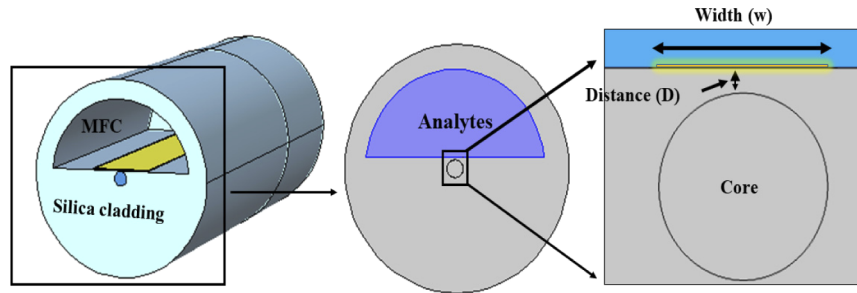

Fig. 1. Cross-sectional view of the proposed sensor design

The channel position (D) is initially considered to be 1.3 μm above the core with an Au strip of thickness (t_{Au}) and width (w) of 0.035 μm and 10 μm, respectively, deposited on the base of MFC. Later, the MFC is filled with analytes (n_a) of different RI. The RI of Au is calculated by the Lorentz-Drude model [32]. The deposition of smooth gold film at the base of channel can be performed by high pressure deposition technique reported by Sazio and Badding [33] and Baril *et al.* [34]. In which the deposition rate, the t_{Au} of the film can be controlled precisely by controlling the deposition time, and the width (w) of the Au strip can be controlled by limiting the deposition area. After the fabrication of sensor, it can be filled by using traditional method used to fill the PCF fibers of varying hole size [30]. The most intuitive way to fill the MFC with analyte is capillarity. In which one end of the sensor will be immersed in liquid while the other end will be left open at room pressure. Here, The designed sensor is modelled and characterized by COMSOL multiphysics, which is based on a full-vectorial FEM [35,36].

Figure 2 illustrates the experimental setup of designed sensing system which can be used to validate our numerical analysis. The setup contains a white light source with optical spectrum analyzer (OSA) to monitor the output response propagated through proposed sensor. Both ends of proposed sensor are spliced with SMF of diameter 125 μm using fusion splicer and the liquid is considered to be sealed in the MFC of designed sensor. This configuration of sensing system using all-in-fiber shows the strong mechanical reliability and easy to operate in remote sensing. In general, the conventional optical fibers are modified to confine the propagating light inside the core, which is in direct contact with the external medium and hence work as a sensor [37]. Now, in proposed sensor the part of the cladding of the fiber is replaced by an MFC incorporating the measurand and an Au strip for the sensing application. When the light is launched in the sensor its fundamental or core guided mode propagates along the length of device and excite the surface plasmons at metal dielectric interface. Now, when the propagation constant of the excitation photons matches with the electron oscillations at a certain wavelength, also known as resonance wavelength, SPR phenomenon occurs, where the part of the energy of the incident light is transferred to the surface plasmons. Then the specific effective refractive index (n_{eff}) of the measurand is monitored for the characteristics of the transmission light.

The aim of the designed sensor is to make a cost effective and highly sensitive sensing device which can be capable for multiple parameters sensing such as chemical, physical and biological sensing. The main advantage of the proposed sensor is in its design. Here we have incorporated an MFC just above the core as it gives more sensitivity in comparison to earlier reported articles and also minimize the wastage of analytes as it required only small amount of measurand to be
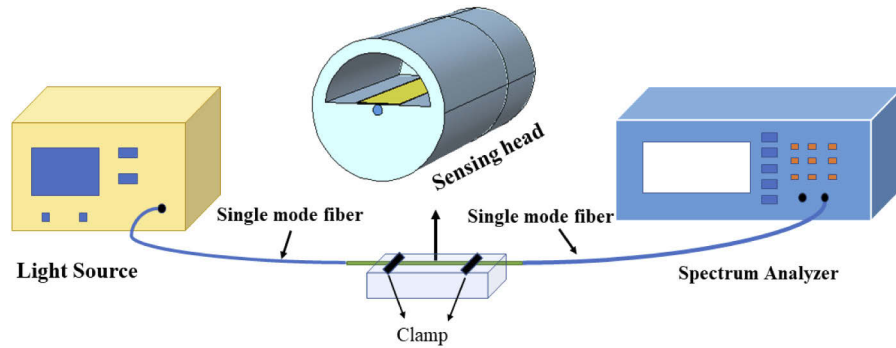
Fig. 2. Schematic diagram of experimental setup for designed sensor system

detected. The used Au strip also have their salient feature in sensing as the metal is chemically inert, long-term stable, biocompatible, and they also don't not suffer oxidation issue. Due to all these feature the proposed sensing device can be used effectively in chemical and biological sensing.

3. Result and discussion

The dispersion relation between core guided mode and surface plasmon polaritons (SPP) mode is shown in Fig. 3. Here we observed a strong birefringence between the core mode and plasmonic mode due to asymmetrical SPR region. The plot shows the real effective index ($Re(n_{eff})$) of core guided mode and SPP mode at different wavelengths and the loss spectra of the designed sensor. It can be observed here that the $Re(n_{eff})$ of SPP mode shown by a black dotted line decreases linearly while the $Re(n_{eff})$ of core guided mode shown by red dotted line remains almost constant with the variation of wavelength, but with a small kink near the mode coupling position. Figure shown in insets illustrates the electric field distribution of core mode, SPP mode and phase matched at $n_a = 1.33$ for the optimized parameters of the designed sensor. The plasmonic mode with most of the power confined in the Au strip shown as the top upset. On the other hand, left inset shows most of the power inside the fiber core. The wavelength, at which the phase matching between two modes takes place, is known as the resonating wavelength. For the proposed sensor, most of the electromagnetic field extends into the cladded region with the increasing wavelength, which leads the reduction of $Re(n_{eff})$. The fields on the left and right sides of resonance wavelength are known as slow and fast electromagnetic fields, respectively. This electromagnetic field is accelerated and deaccelerated by resonance, therefore the appearance of kink near resonance wavelength takes place [30,38]. The inset-on right shows degenerated mode field coupling both the core and plasmonic modes. Although field intensity in the upper metal layer is stronger but core with a larger area contains similar amount of power. The modal loss of the designed sensor is calculated from the imaginary part of effective index by following relation [39]

$$\alpha \left(\frac{dB}{m} \right) = 8.686.k_0.\, Im(n_{eff}) \tag{2}$$

where the wavenumber (k_0) is defined as $k_0 = 2\pi/\lambda$. The plasmonic mode is very lossy compared to the dielectric core mode. So, when the core mode gets mixed with plasmonic mode close to the resonance wavelength (λ_R), its loss value very sharply increased, as shown by the blue dotted line.

In the numerical simulations, we have first investigated the influence of structural parameter before characterizing the sensor for various refractive index ranges. The distance (*D*) of MFC
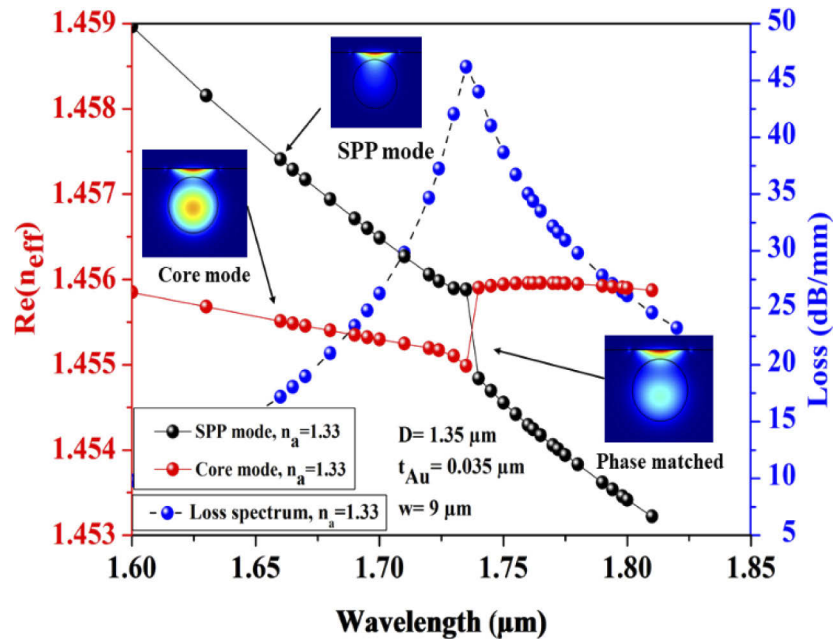
Fig. 3. Dispersion curves of the core and SPP modes for n_a=1.33. Inset mode profile shows the electric field distribution for proposed sensor at λ=1.66 μm and the phase matching profile at λ_R = 1.735 μm.

from the core, plays the most important role in the maximum coupling of core guided mode and SPP mode. Since, the absence of *D* will make the sensor as conventional fiber and the propagated light will never come in direct contact of analytes hence it requires the polishing and optimization of *D* to achieve a high sensitivity of the sensing device. While investigating the effect of *D* over the sensing response, the other parameters like t_{Au}, *w* and n_a are kept constant throughout the optimization process. Figure 4 (a) exhibits the optimization of *D* with respect to variation in wavelength. We have varied *D* from 1.2 μm to 1.5 μm to optimize the distance of channel from the core. Such separation of MFC from the core can be achieved by the mechanical method, as previously reported article [28]. Here, we can clearly observe that the maximum modal loss of 42.87 dB/mm is obtained for D = 1.35 μm at 1.652 μm while 37.19 dB/mm, 39.35 dB/mm, 41.19 dB/mm, 40.87 dB/mm, 29.88 dB/mm, and 24.76 dB/mm are obtained for *D* = 1.2 μm, 1.25 μm, 1.3 μm, 1.4 μm, 1.45 μm, and 1.5 μm, respectively, with blue shifting in the resonance wavelength. Figure 4 (b) shows the influence of variation of separation between core and the MFC. We can clearly observe the blue shifting and the corresponding peak loss in Fig. 4 (b) with the distance, *D*. initially, the peak loss value increases continuously till D = 1.35 μm, thereafter, a smooth decrease in peak loss takes place for D = 1.40 μm and beyond of that, the peak loss value is fallen sharply at D = 1.50 μm. The encircled points illustrate the maximum loss and their corresponding separation of MFC from the core. The variation in loss spectra may take place due to the fact that the interaction region of electric field of core mode at metal dielectric interface is more at optimized *D* because of spreading of the field, as *D* increases the metal-dielectric interface reach far away from the core and hence the strength of electric field is quite small which may results in the decrease in modal loss.

The maximum loss spectrum can only appears due to the presence of the Au strip of optimized thickness and width as it is also acting as a lossy waveguide. The lossy plasmonic mode guided by an Au strip forms a supermode when it placed close to the fibre core. As a result, the fibre
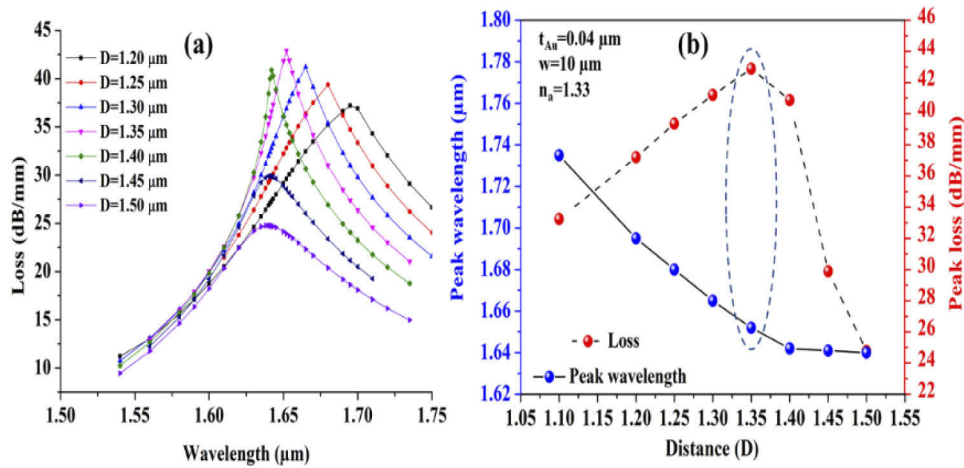
Fig. 4. (a). Variation in loss spectra at various separations (*D*) between MFC and core, (b). influence of variation of *D* over modal loss.

transmission shows a peak in the loss spectra where both the plasmonic and dielectric modes get phase matched and form a supermode. The peak of the loss spectra may be sharp or wide depending on the thickness and width of Au strip. It is well known that the plasmons are formed at the outer surface of a metal. Therefore, a thicker Au satisfy the phase matching condition and results in a wider peak in the loss spectra. On the other hand, a thin Au strip follows a strong coupling with the fibre core mode, resulting in a much sharper peak in the loss spectra. Hence, it requires the optimization of thickness and width Au strip to achieve strong coupling and sharper peak in loss spectra for high sensitivity of the sensing device.

Figure 5 illustrates the confinement loss spectra of the fundamental mode for different Au thickness (t_{Au}). Here, from Fig. 5 (a) we can see the strong influence of thickness on the loss spectra. To optimize the thickness of Au strip we have performed the analysis for $t_{Au} = 0.025\,\mu m$, $0.030\,\mu m$, $0.035\,\mu m$, $0.040\,\mu m$, and $0.045\,\mu m$ and these show the maximum modal loss of $42.12\,dB/mm$, $42.92\,dB/mm$, $43.16\,dB/mm$, $42.87\,dB/mm$, and $41.82\,dB/mm$, respectively. From the obtained trend of modal loss, we can clearly observe that when the thickness of Au is increased from $0.025\,\mu m$ to $0.035\,\mu m$, the peak wavelength continuously decreases throughout the variation of thickness while the peak loss increases up to $t_{Au} = 0.035\,\mu m$ and then decreases with an evident of blue shifting in loss spectra varying from $\lambda_R = 2.26\,\mu m$ to $1.573\,\mu m$. In addition to blue shift, we also obtained a smaller full width at half-maxima (FWHM) and higher loss among the other curves which suggests that Au of thickness $0.035\,\mu m$ can the optimum value for the proposed sensor. Moreover, the influence of the Au thickness variation on the proposed structure is shown in Fig. 5 (b). Here, we have shown the variation of peak wavelength and spectral loss with the thickness of Au. We can clearly observe the blue shift in loss spectra with maximum modal loss of $43.16\,dB/mm$ is obtained at $\lambda_R = 1.775\,\mu m$, shown by encircled region in Fig. 5 (b).

After optimization of the thickness, the influence of Au strip width (*w*) is studied to obtain the optimum width. Figure 6 (a) shows the spectral loss for $w = 8\,\mu m$, $8.5\,\mu m$, $9\,\mu m$, $9.5\,\mu m$, and $10\,\mu m$, keeping other parameters unchanged. Here, we can clearly observe the resonant wavelength are shifting towards the longer wavelength increasing from $1.7\,\mu m$ to $1.775\,\mu m$, which illustrate a considerable red shift of the loss spectra with the increase in Au width. As the width reaches to $9\,\mu m$ we observed a maximum modal loss of $46.20\,dB/mm$ at $\lambda_R = 1.735\,\mu m$. Figure 6 (b) clearly shows the effect of width on the resonance wavelength and the peak modal loss. This graph illustrates that with the increasing width, first, the loss increases untill $w = 9\,\mu m$ than start
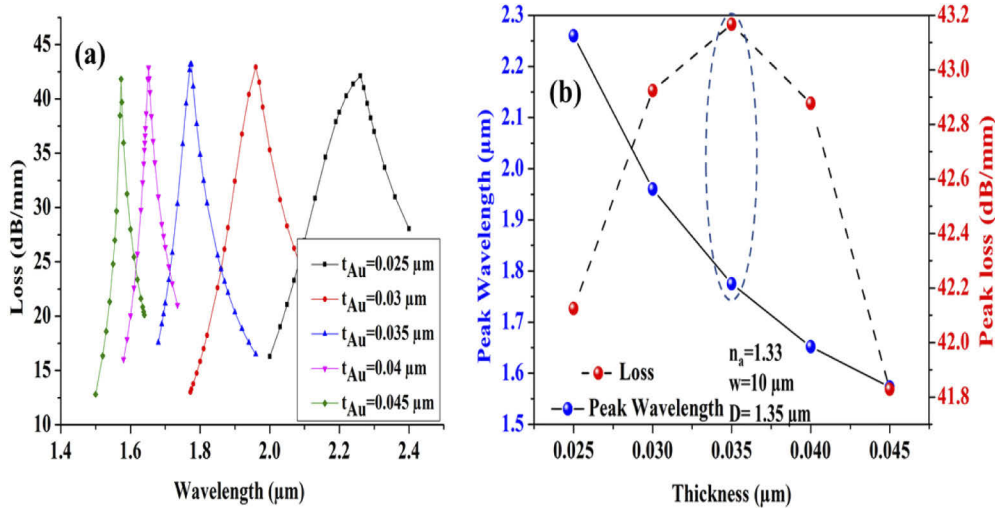
Fig. 5. (a) Variation in loss spectra at different t_{Au} with respect to wavelength, (b) influence of variation of Au thickness (t_{Au}) over modal loss.

decreasing beyond that. The points encircled in Fig. 6 (b) shows the maximum loss for 9 μm and this may be considered as an optimized width of the Au strip width.
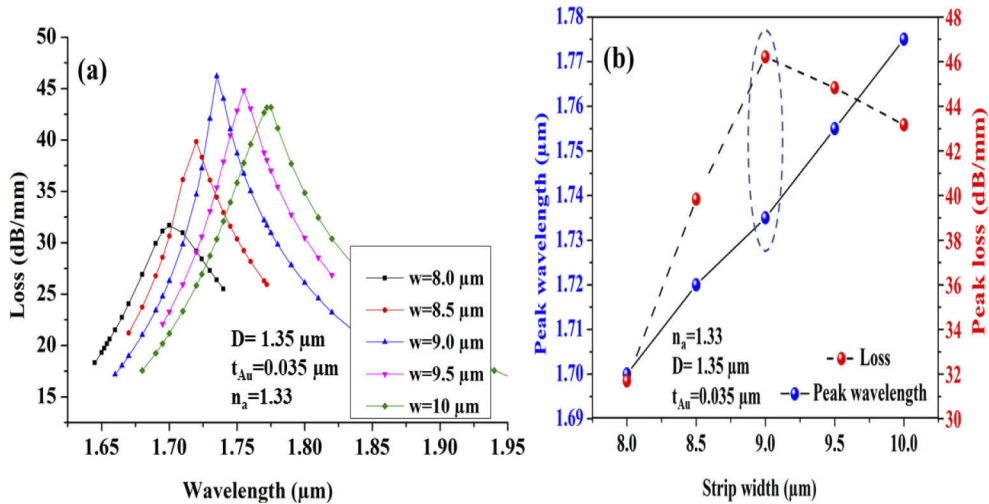

Fig. 6. (a) Variation in loss spectra at different width of Au strip and (b). variation of the peak wavelength and the loss with the Au width.

Further, after optimization of all the parameters, the proposed sensor is characterized for a wide range of n_a varying between 1.33 to 1.43. The variation of loss spectra with the wavelength for different n_a values shown in Fig. 7 (a) illustrates the red shift in resonance wavelength with the variation of n_a. Here, we can see the FWHM of resonance peak getting broaden with the increasing n_a. The broadening of resonance peak is arising due to comparative lower index contrast due to increasing n_a. Figure 7 (b) illustrates the variation in λ_R corresponding to the variation of n_a. It is obvious that the shift in the peak of λ_R will take place with the increase in n_a as shown in figure. The numerically simulated data points shown in Fig. 7 (b) are obtained

from the spectral loss shown in Fig. 7 (a) and fitted by a 3rd order polynomial. From Fig. 7 (b), a nonlinear variation is observed towards the red shift in resonance wavelength with respect to n_a varied from $\lambda_R = 1.735\,\mu m$ to $2.09\,\mu m$ while for range $n_a = 1.41\text{-}1.43$ we have obtained a linear response of the sensor as shown by Fig. 7 (b) with a maximum wavelength shift of $\Delta\lambda = 1.65\,\mu m$.
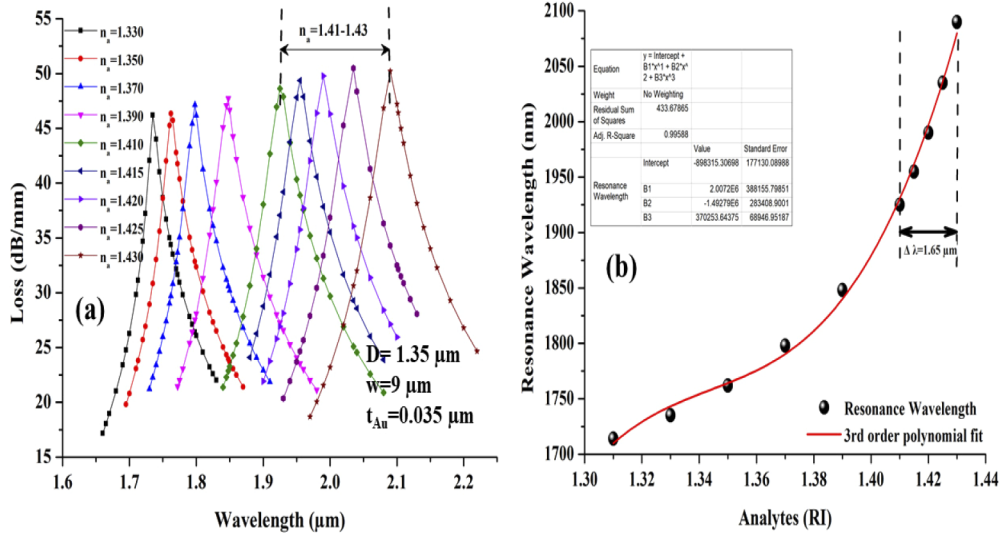

Fig. 7. Variation of (a) loss spectra and (b). resonance wavelength, at different n_a.

The sensitivity of the proposed sensor, defined as the change in resonance wavelength divided by change in n_a, is obtained by the wavelength interrogation technique and is calculated by following relation [39].

$$S = \frac{\Delta\lambda_{peak}}{\Delta n_a} \left(\frac{nm}{RIU}\right) \qquad (3)$$

where $\Delta\lambda_{peak}$ and Δn_a, represent the change in resonance wavelength and change in n_a, respectively. Figure 8 illustrates the calculated sensitivity of the sensor with respect to varying n_a. Table 1 shows the sensitivity corresponding to the different n_a varying from 1.33 to 1.43. We have also calculated its figure of merits (FOM) to select the optimal range of RI. The FOM may be defined as the ratio of FWHM with the sensitivity of the designed sensor [40]

Table 1. Device sensitivity and FOM corresponding to each n_a

Analytes (RIU)	Resonance Wavelength (nm)	Resonance peak shift (nm)	Sensitivity (nm/RIU)	FWHM	FOM (1/RIU)
1.33	1735	27	1350	145	9.31
1.35	1762	36	1800	154	11.68
1.37	1798	50	2500	170	14.70
1.39	1848	80	3850	186	20.69
1.41	1925	165	8250	207	39.85
1.43	2090	–	–	–	–

The proposed sensor is optimized for its all parameters to achieve a high sensitivity. By observing each range and their respective sensitivity we can clearly observe that the S increases with the increasing n_a. The average sensitivity of 8250 nm/RIU is obtained for sensing range $n_a = 1.41\text{-}1.43$, however beyond of this we have varied n_a over a small range around 1.415,
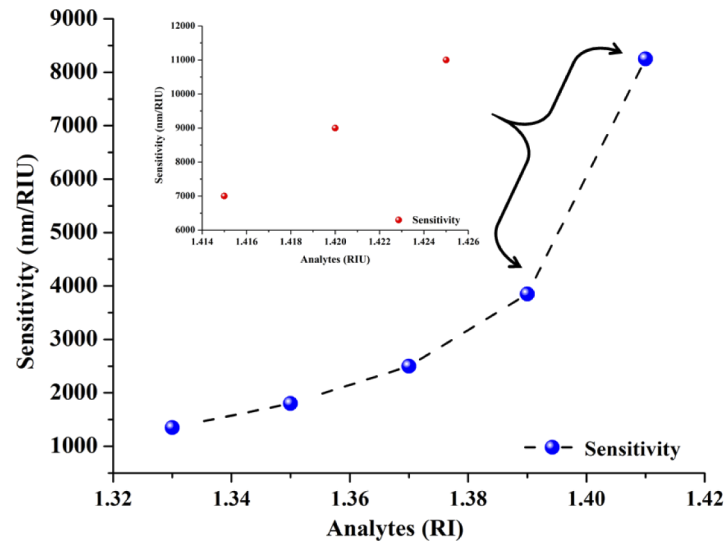
Fig. 8. Sensitivity variation with the measurand refractive index (n_a).

1.420, and 1.425 and obtained the maximum sensitivity of 7000 nm/RIU, 9000 nm/RIU, and 11000 nm/RIU, respectively, shown in inset of Fig. 8. The highest sensitivity in small variation of analytes illustrate that our sensor can work effectively even with small variation and high RI of measurand. Table 2 compares our work with other reported sensitivity according to their sensing range.

Table 2. The detailed comparison of various sensors and their sensitivity.

Sensing structure	Sensitivity (nm/RIU)	Sensing range
D-shaped PCF with nanoscale belt	3751.5 [41]	1.20-1.40
D-shaped photonic crystal fiber (PCF)	7381 [25]	1.40-1.42
Plasmonic sensor using Niobium nanofilm	8000 [27]	1.40
SPR sensor based on D-shaped MFC (our design)	8250	1.41-1.43
	11000	1.425-1.43

4. Conclusion

In conclusion, we have designed a novel SPR sensor using D-shaped MFC. The sensor is analyzed by using a full-vectorial FEM technique on COMSOL multiphysics because of its high accuracy and less computational time. The sensor is based on wavelength interrogation method. The structural parameters such as D, t_{Au}, and w, are optimized through numerical simulations to achieve higher sensitivity. In the designed sensor we have reported the continuous increment in sensitivity with increasing n_a from 1.33 to 1.43. Our proposed sensor has shown the average device sensitivity of 8250 nm/RIU in the sensing range $n_a = 1.41$-1.43. For more accurate result in this range we have varied the n_a in small steps of 0.005 and obtained the maximum sensitivity of 7000 nm/RIU, 9000 nm/RIU, and 11000 nm/RIU for $n_a = 1.415$, 1.420, and 1.425, respectively. The results indicate that the proposed sensor is not only achieving high sensitivity but also open up other ways to fabricate sensors for other sensing applications using similar or modified structures.

Acknowledgment

References

1. B. Prabowo, A. Purwidyantri, and K.-C. Liu, "Surface plasmon resonance optical sensor: A review on light source technology," Biosensors **8**(3), 80 (2018).
2. C. Caucheteur, T. Guo, and J. Albert, "Review of plasmonic fiber optic biochemical sensors: improving the limit of detection," Anal. Bioanal. Chem. **407**(14), 3883–3897 (2015).
3. A. K. Sharma, A. K. Pandey, and B. Kaur, "A review of advancements (2007–2017) in plasmonics-based optical fiber sensors," Opt. Fiber Technol. **43**, 20–34 (2018).
4. H. Nguyen, J. Park, S. Kang, and M. Kim, "Surface plasmon resonance: a versatile technique for biosensor applications," Sensors **15**(5), 10481–10510 (2015).
5. M. H. Elshorbagy, A. Cuadrado, and J. Alda, "High-sensitivity integrated devices based on surface plasmon resonance for sensing applications," Photonics Res. **5**(6), 654–661 (2017).
6. A. K. Pathak, D. K. Chaudhary, and V. K. Singh, "Broad range and highly sensitive optical pH sensor based on Hierarchical ZnO microflowers over tapered silica fiber," Sens. Actuators, A **280**, 399–405 (2018).
7. F. Xiao, D. Michel, G. Li, A. Xu, and K. Alameh, "Simultaneous measurement of refractive index and temperature based on surface plasmon resonance sensors," J. Lightwave Technol. **32**(21), 4169–4173 (2014).
8. E. Kretschmann and H. Raether, "Notizen: radiative decay of non radiative surface plasmons excited by light," Zeitschrift für Naturforsch. A **23**(12), 2135–2136 (1968).
9. S. Kumari and S. Gupta, "Cladding stress induced performance variation of silicon MMI coupler," Photonics Nanostructures - Fundam. Appl. **33**, 55–65 (2019).
10. S. Ghosh and B. M. A. Rahman, "A compact Mach–Zehnder interferometer using composite plasmonic waveguide for ethanol vapor sensing," J. Lightwave Technol. **35**(14), 3003–3011 (2017).
11. C. Liu, L. Yang, Q. Liu, F. Wang, Z. Sun, T. Sun, H. Mu, and P. K. Chu, "Birefringent PCF based SPR sensor for a broad range of low refractive index detection," IEEE Photonics Technol. Lett. **30**(16), 1471–1474 (2018).
12. D. F. Santos, A. Guerreiro, and J. M. Baptista, "Surface plasmon resonance sensor based on D-type fiber with a gold wire," Optik **139**, 244–249 (2017).
13. Z. Tan, X. Li, Y. Chen, and P. Fan, "Improving the sensitivity of fiber surface plasmon resonance sensor by filling liquid in a hollow core photonic crystal fiber," Plasmonics **9**(1), 167–173 (2014).
14. J. K. Nayak and R. Jha, "Numerical simulation on the performance analysis of a graphene-coated optical fiber plasmonic sensor at anti-crossing," Appl. Opt. **56**(12), 3510–3517 (2017).
15. M. Hasan, S. Akter, A. Rifat, S. Rana, and S. Ali, "A highly sensitive gold-coated photonic crystal fiber biosensor based on surface plasmon resonance," Photonics **4**(4), 18 (2017).
16. A. A. Rifat, R. Ahmed, A. K. Yetisen, H. Butt, A. Sabouri, G. A. Mahdiraji, S. H. Yun, and F. R. M. Adikan, "Photonic crystal fiber based plasmonic sensors," Sens. Actuators, B **243**, 311–325 (2017).
17. A. Gowri and V. V. R. Sai, "Development of LSPR based U-bent plastic optical fiber sensors," Sens. Actuators, B **230**, 536–543 (2016).
18. X. Dong, H. Y. Tam, and P. Shum, "Temperature-insensitive strain sensor with polarization-maintaining photonic crystal fiber based Sagnac interferometer," Appl. Phys. Lett. **90**(15), 151113 (2007).
19. J. H. Osório, G. Chesini, V. A. Serrão, M. A. R. Franco, and C. M. B. Cordeiro, "Simplifying the design of microstructured optical fibre pressure sensors," Sci. Rep. **7**(1), 2990 (2017).
20. A. Patnaik, K. Senthilnathan, and R. Jha, "Graphene-based conducting metal oxide coated D-shaped optical fiber SPR sensor," IEEE Photonics Technol. Lett. **27**(23), 2437–2440 (2015).
21. H. Qazi, A. Mohammad, H. Ahmad, and M. Zulkifli, "D-shaped polarization maintaining fiber sensor for strain and temperature monitoring," Sensors **16**(9), 1505 (2016).
22. M. H. Cordaro, D. L. Rode, T. S. Barry, and R. R. Krchnavek, "Precision fabrication of D-shaped single-mode optical fibers by in situ monitoring," J. Lightwave Technol. **12**(9), 1524–1531 (1994).
23. Y. Al-Qazwini, A. S. M. Noor, Z. Al-Qazwini, M. H. Yaacob, S. W. Harun, and M. A. Mahdi, "Refractive index sensor based on SPR in symmetrically etched plastic optical fibers," Sens. Actuators, A **246**, 163–169 (2016).
24. J. M. Kvavle, S. M. Schultz, and R. H. Selfridge, "Low loss elliptical core D-fiber to PANDA fiber fusion splicing," Opt. Express **16**(18), 13552–13559 (2008).
25. Q. Xie, Y. Chen, X. Li, Z. Yin, L. Wang, Y. Geng, and X. Hong, "Characteristics of D-shaped photonic crystal fiber surface plasmon resonance sensors with different side-polished lengths," Appl. Opt. **56**(5), 1550–1555 (2017).
26. N. Luan, C. Ding, and J. A. Yao, "Refractive Index and temperature sensor based on surface plasmon resonance in an exposed-Core microstructured optical fiber," IEEE Photonics J. **8**(2), 1–8 (2016).
27. M. R. Hasan, S. Akter, K. Ahmed, and D. Abbott, "Plasmonic refractive index sensor employing niobium nanofilm on photonic crystal fiber," IEEE Photonics Technol. Lett. **30**(4), 315–318 (2018).
28. G. An, S. Li, T. Cheng, X. Yan, X. Zhang, X. Zhou, and Z. Yuan, "Ultra-stable D-shaped optical fiber refractive index sensor with graphene-gold deposited platform," Plasmonics **14**(1), 155–163 (2019).

29. L. Li, G. Wylangowski, D. N. Payne, and R. D. Birch, "Broadband metal/glass single-mode fibre polarisers," Electron. Lett. **22**(19), 1020 (1986).

30. S. Weng, L. Pei, J. Wang, T. Ning, and J. Li, "High sensitivity D-shaped hole fiber temperature sensor based on surface plasmon resonance with liquid filling," Photonics Res. **5**(2), 103–107 (2017).

31. V. Brucker, "To the use of Sellmeier formula," Springer, pp. 0–7, 2011.

32. A. D. Rakić, A. B. Djurišić, J. M. Elazar, and M. L. Majewski, "Optical properties of metallic films for vertical-cavity optoelectronic devices," Appl. Opt. **37**(22), 5271–5283 (1998).

33. P. J. A. Sazio, A. Correa, C. F. Finlayson, J. R. Hayes, T. J. Scheidemantel, N. F. Baril, B. R. Jackson, D.-J. Won, F. Zhang, E. R. Margine, V. Gopalan, V. H. Crespi, and J. V. Badding, "Microstructured optical fibers as high-pressure microfluidic reactors," Science **311**(5767), 1583–1586 (2006).

34. R. He, T. D. Day, J. R. Sparks, B. Keshavarzi, M. Krishnamurthi, A. Borhan, V. Gopalan, A. C. Peacock, N. Healy, P. J. A. Sazio, and J. V. Badding, "Confined high-pressure chemical deposition of hydrogenated amorphous silicon," J. Am. Chem. Soc. **134**(1), 19–22 (2012).

35. B. M. A. Rahman and J. B. Davies, "Finite-element analysis of optical and microwave waveguide problems," IEEE Trans. Microwave Theory Tech. **32**(1), 20–28 (1984).

36. "COMSOL Multiphysics® Modeling Software."

37. Y. S. Dwivedi, A. K. Sharma, and B. D. Gupta, "Influence of design parameters on the performance of a surface plasmon sensor based fiber optic sensor," Plasmonics **3**(2-3), 79–86 (2008).

38. Z. Tan, X. Hao, Y. Shao, Y. Chen, X. Li, and P. Fan, "Phase modulation and structural effects in a D-shaped all-solid photonic crystal fiber surface plasmon resonance sensor," Opt. Express **22**(12), 15049–15063 (2014).

39. A. K. Pathak, S. Ghosh, R. K. Gangwar, B. M. A. Rahman, and V. K. Singh, "Metal nanowire assisted hollow core fiber sensor for an efficient detection of small refractive index change of measurand liquid", Plasmonics, doi:10.1007/s11468-019-00969-y (in Press), 2019.

40. E. Klantsataya, P. Jia, H. Ebendorff-Heidepriem, T. Monro, and A. François, "Plasmonic fiber optic refractometric sensors: from conventional architectures to recent design trends," Sensors **17**(12), 12–23 (2016).

41. W. Zhang, Z. Lian, T. Benson, X. Wang, and S. Lou, "A refractive index sensor based on a D-shaped photonic crystal fiber with a nanoscale gold belt," Opt. Quantum Electron. **50**(1), 29 (2018).